Two-dimensional spin-polarized fermion lattice gases

J. E. Gubernatis
Center for Materials Science, Los Alamos National Laboratory, Los Alamos, New Mexico 87545

D. J. Scalapino and R. L. Sugar
Department of Physics and Institute for Theoretical Physics, University of California, Santa Barbara, California 93106

W. D. Toussaint
Department of Physics, University of California, San Diego, La Jolla, California 92093
(Received 31 October 1984)

A model of spin-polarized fermions hopping on a two-dimensional lattice with a nearest-neighbor interaction V is studied. Random-phase-approximation calculations predict that the half-filled system undergoes a density-wave transition for positive values of V, an odd-angular-momentum pairing transition for small negative V, and a condensation-phase-separation transition for more negative values of V. The classical lattice-gas Ising limit matches onto the density-wave transition for $V>0$ and the condensation transition for $V<0$. A strong-coupling expansion in powers of the ratio of single-fermion transfer-matrix element t to the two-body interaction V provides the leading corrections to the Ising limit. In order to explore the intermediate-coupling regime, fermion Monte Carlo calculations were carried out and various Green's functions characterizing the quantum correlations evaluated. With use of finite-size scaling techniques, the density-wave and condensation phase boundaries were followed into the intermediate-coupling regime. At these transitions, measured quantities scaled well with the usual Ising indices. Unfortunately, the weak-coupling regime lies beyond the reach of these simulations, and we conclude that a method suitable for the weak-coupling regime is needed to complete the phase diagram.

I. INTRODUCTION

The classical lattice gas (Ising model) studied by Lee and Yang[1] has provided useful insight into the order-disorder condensation phenomena of classical gases. Here we consider the quantum version of this lattice gas in which a near-neighbor single-particle overlap integral t (hopping term) is added to the classical two-particle near-neighbor interaction V. The particles are assumed to obey Fermi statistics and to be fully spin polarized. Thus, since only one spin orientation is considered, the fermions are effectively spinless. Submonolayer films of spin-polarized $^3He_\downarrow$ or metastable $D_\downarrow$ adsorbed on substrates represent possible realizations of such two-dimensional fermion lattice gases.

We have used several different approaches to gain insight into the properties of such systems. In Sec. II we begin by discussing perturbation theory and RPA approximations for $|V|/t<1$. Then the strong-coupling regime $V/t\gg 1$ is discussed using results obtained from high-temperature-series expansions of the anisotropic spin-$\frac{1}{2}$ Heisenberg model.[2] In Sec. III we use recently developed quantum Monte Carlo techniques[3,4] and a finite-size scaling analysis[5] to explore the intermediate-coupling regime. This is followed by a brief conclusion in Sec. IV and an Appendix in which the fermion Monte Carlo procedure we use is outlined. In the remainder of this Introduction, we discuss the model and summarize some of our results.

The model we study has a Hamiltonian

$$H=\sum_{\langle ij\rangle}[-t(c_i^\dagger c_j+c_j^\dagger c_i)+V(n_i-\tfrac{1}{2})(n_j-\tfrac{1}{2})]\ , \qquad (1)$$

with $i=(i_x,i_y)$ and $j=(j_x,j_y)$ nearest-neighbor points on a square lattice. The second term proportional to V is just the usual classical lattice-gas model, and the first term is the kinetic energy arising from the single fermion transfer integral t between sites. The $c_i^\dagger$ and c_j operators create and destroy fermions on the ith and jth sites, respectively. These operators obey the usual fermion anticommutation relations

$$\{c_i,c_j^\dagger\}=\delta_{ij}\ , \qquad (2)$$

and $n_i=c_i^\dagger c_i$ is the occupation-number operator for the ith site. Here we focus on the half-filled case in which on the average a finite-size lattice has half as many fermions as sites. Thus, we have written Eq. (1) in a particle-hole symmetric form.

In this lattice problem, the quantum parameter is t/V, which is proportional to the square of de Boer's[6] well-known quantum parameter. We find it convenient to work in units where $t=1$. Thus, for $|V|\gg 1$, the quantum parameter is small, and the system becomes classical. In this limit, since the half-filled case corresponds to zero magnetic field for the Ising model, an order-disorder transition occurs when[7] $\sinh(|V|/kT_c)=1$ ($T_c=0.56|V|$). For large positive V the ordered state is characterized by a staggered site density on two interpenetrating A-B sublattices (an antiferromagnetic Ising phase). For a large at-

tractive interaction, the transition corresponds to the usual (Ising ferromagnetic) gas-liquid condensation.

The phase diagram is schematically illustrated in Fig. 1, which shows the transition temperature versus the interaction potential measured in units of t. We use the notation T_{DW} for the temperature of the density-wave transition, T_{TP} for the triplet-pairing transition, and T_{con} for the condensation transition. The straight dashed lines correspond to the Ising result $0.56\,|\,V\,|$, and the lattice illustrations show one of the characteristic low-temperature broken-symmetry phases. In the large-V limit, the onset of order is continuous with the usual two-dimensional (2D) Ising indices. As V decreases, we move into the quantum regime and new phenomena occur.

From our studies described below, we find that the T-V phase diagram including the quantum regime looks like the solid curves shown in Fig. 1. For nonzero values of t, the ordered phase of the system is a $2p_F$ density wave which becomes the usual staggered density phase of the Ising model when $V \gg t$. As V goes to zero, a random-phase-approximation (RPA) calculation gives $T_{\mathrm{DW}} \sim \exp(-\pi/\sqrt{V})$. This suggests that the phase boundary continues into the origin. However, fluctuations may alter this behavior, causing T_{DW} to vanish below a critical value of V. We indicate this uncertainty by the short-dashed part of the curve. Further work is needed to construct a reliable weak coupling solution.

For negative values of V, the RPA calculations predict that, at small values of V and low temperatures, $T_{\mathrm{TP}} \sim \exp(-2\pi/\sqrt{V})$, the system condenses into a pairing state which is a superposition of odd angular-momentum states. Again, fluctuation effects may entirely wash out this phase and certainly at best the system can have only a Kosterlitz-Thouless—like[8] transition to a topologically ordered state with no long-range order because of phase fluctuations in this 2D system. In Fig. 1 this phase is indicated by the narrow shaded region labeled by TP for triplet pairing, which is appropriate if we think of the fermion system as spin polarized. The phase boundary is again indicated by the dashed line because it occurs in a parameter regime which we are unable to reach with our present Monte Carlo techniques. At larger values of V, the usual condensation transition occurs, and from the strong-coupling analysis of Sec. III we find that initially T_{con} deviates from the Ising result as

$$T_{\mathrm{con}} \cong 0.56\,|\,V\,|\left[1-\frac{1}{V^2}\right] . \tag{3}$$

Just as for $V>0$, we argue that this transition is Ising-like. We are uncertain as to how the competition between the condensation and pairing phases is resolved. In the XXZ Heisenberg model, the transition temperature of the Ising-like phase transition for $J_z \geq J_x$ and the Kosterlitz-Thouless XY-like transition for $J_z \leq J_x$ both vanish at the isotropic $J_z = J_x$ point. However, we have not found a corresponding symmetry argument for the fermion problem, and the resolution of the low-temperature part of the phase diagram for negative V also awaits the development of a reliable weak-coupling theory.

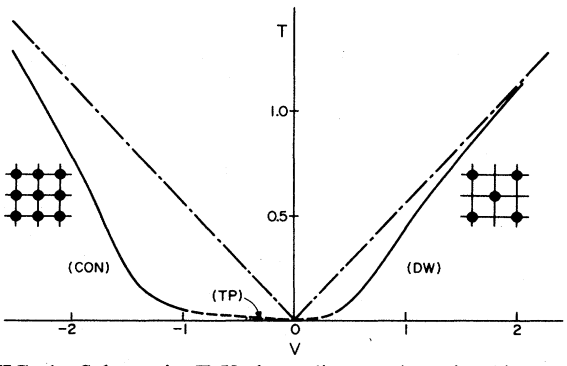

FIG. 1. Schematic T-V phase diagram in units where $t=1$. The straight long-dashed—short-dashed lines correspond to the Ising result appropriate for $|\,V\,| \gg 1$. The solid lines denote the phase boundaries for the density-wave ($V>0$) and condensation ($V<0$) transitions. The region labeled TP denotes an odd angular-momentum triplet-pairing phase, but fluctuations may wash out the phase transition at weak coupling, and we indicate our uncertainty by drawing the phase boundaries with dashed lines in the weak-coupling regime. We expect that if the TP phase occurs, it exists only at significantly lower temperatures than indicated in this schematic.

II. PERTURBATION THEORY AND STRONG-COUPLING APPROXIMATIONS

As we noted, the strong-coupling limit $|\,V\,| \gg 1$ of our model corresponds to the Ising model. The extreme weak-coupling limit $V=0$ corresponds to a half-filled band of noninteracting fermions. Expressing the Hamiltonian equation (1) in terms of momentum eigenstates we have

$$H = \sum_p \epsilon_p c_p^\dagger c_p + \frac{1}{2N}\sum_{p,k,q} V(q) c_{p+q}^\dagger c_{k-q}^\dagger c_k c_p . \tag{4}$$

Here the band energy in units where $t=1$ is

$$\epsilon_p = -2(\cos p_x + \cos p_y) - V , \tag{5}$$

and

$$V(q) = 2V(\cos q_x + \cos q_y) . \tag{6}$$

There are two special features of the noninteracting $V=0$ problem which play essential roles in the response of the system. First, the Fermi surface of the noninteracting problem, shown in Fig. 2, has perfect nesting for the creation of a particle-hole pair with momentum transfers $2p_F = \pm(\pm\pi,\pi)$. This gives rise to a low-temperature divergence in the density-density susceptibility. Secondly, for this near-neighbor hopping model, the single-particle density of states in the continuum limit has a logarithmic Van Hove[9] singularity at the Fermi surface of the half-filled band:

$$N(\omega) = \frac{1}{N}\sum_p \delta(\omega-\epsilon_p) = \frac{1}{2\pi^2} K\left[1-\left|\frac{\omega}{4}\right|^2\right] , \tag{7}$$

with K the complete elliptic integral of the first kind. As $\omega \to 0$, this diverges as

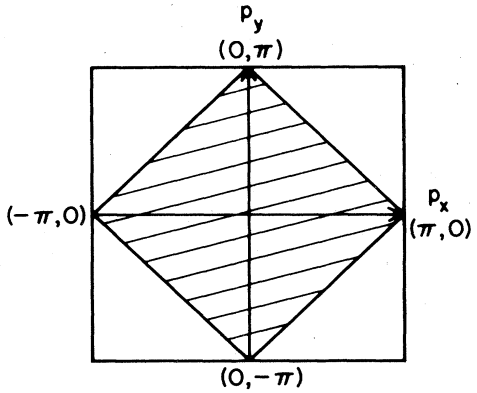

FIG. 2. 2D Fermi surface for our half-filled model.

$$N(\omega)\cong\frac{1}{2\pi^2}\ln(16/|\omega|)\ . \tag{8}$$

This is actually a good approximation over the entire band $|\omega|\leq 4$. The zero-frequency density-density susceptibility at $q=0$ is proportional to $N(kT)$, so that the noninteracting fermion system is highly compressible. Finally, we will find that the $q=0$ limit of the neighbor pair-pair susceptibility (triplet pairing if we think of the fully polarized system)

$$P(q)=\int_0^\beta d\tau\langle\Delta_q(\tau)\Delta_q^\dagger(0)\rangle\ , \tag{9}$$

with

$$\Delta_q^\dagger=\frac{1}{N}\sum_l e^{iql}(c_{l+\hat{x}}^\dagger c_l^\dagger+c_{l+\hat{y}}^\dagger c_l^\dagger)\ , \tag{10}$$

also diverges as $T\to 0$. Here, $\hat{x}$ and $\hat{y}$ are unit vectors in the x and y direction, respectively. Thus, an analysis of the noninteracting $V=0$ system clearly indicates the three types of order that are of interest. For $V>0$, the density response at $2p_F$ is favored, and for $V<0$ we must consider the $q=0$ density response and the triplet-pairing response.

In order to obtain some insight into the type of density instabilities that may occur, we will study the zero-frequency wave-vector-dependent density-density susceptibility

$$\Pi(q)=\int_0^\beta\langle\rho_q(\tau)\rho_q^\dagger(0)\rangle d\tau \tag{11}$$

and evaluate it within the RPA approximation, which sums the diagrams shown in Fig. 3(a). In this case,

$$\Pi_{\rm RPA}(q)=\frac{\Pi_0(q)}{1+V(q)\Pi_0(q)}\ , \tag{12}$$

with $\Pi_0(q)$ the noninteracting particle-hole bubble

$$\Pi_0(q)=\sum_p\frac{f(\epsilon_{p+q})-f(\epsilon_p)}{\epsilon_p-\epsilon_{p+q}}\ . \tag{13}$$

For $q\to 0$ we have, at low temperatures,

$$\Pi_0(0)=\sum_p-\frac{\partial f}{\partial\epsilon}\cong N(kT)\ , \tag{14}$$

which diverges logarithmically as given by Eq. (5). Therefore, for $V<0$ the RPA prediction for the condensation transition temperature $T_{\rm con}$, determined as the temperature at which $\Pi_{\rm RPA}(0)$ of Eq. (12) diverges,

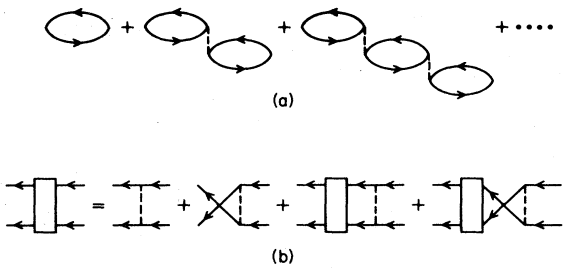

FIG. 3. (a) RPA Feynman graphs for Π, and (b) ladder graphs for the two-particle t matrix.

$$1=4|V|\frac{1}{2\pi^2}\ln(16/T_{\rm con})\ , \tag{15}$$

gives

$$T_{\rm con}=16\exp(-\pi^2/2|V|)\ . \tag{16}$$

For $V>0$, $\Pi_{\rm RPA}(q)$ diverges when $q=2p_F$ and, at low temperatures, we find

$$\Pi_0(2p_F)\cong\frac{1}{2\pi^2}\left[\frac{\ln^2(2/T)}{2}+\ln\left[\frac{16\gamma}{\pi}\right]\ln(2/T)+2.13\right]\ , \tag{17}$$

with $\gamma=1.78$. In this case, within the RPA, the $2p_F$ density-wave state occurs at a transition temperature set by

$$1=4V\Pi_0(2p_F)\ . \tag{18}$$

As $V\to 0$, this gives, for the critical temperature of the density-wave function,

$$T_{\rm DW}=2\exp(-\pi/\sqrt{V})\ . \tag{19}$$

Ordinarily, we would have expected $T_{\rm DW}$ to vary as $\exp[-1/N(0)V]$ with $N(0)$ the single-particle density of states at the Fermi surface. However, as noted, the single-particle density of states for the half-filled system has a logarithmic divergence at the Fermi surface. This, combined with the perfect nesting shown in Fig. 2, produces the $\ln^2(2/T)$ term in Π_0 and leads to the much weaker $\sqrt{V}$ dependence in the exponent of Eq. (19). Hence, the transition occurs at a significantly higher temperature in the weak-coupling regime. This effect, arising from the Van Hove singularity, has the potential for producing interesting physical consequences for other systems, such as the 2D Hubbard[10] model or the 2D electron-exciton model.[11] Finite quasiparticle lifetime effects, of course, ultimately provide a cutoff for the logarithmic 2D Van Hove singularities.

The triplet- or odd angular-momentum-pairing transition temperature $T_{\rm TP}$ can be determined in this same spirit by evaluating the t matrix shown in Fig. 3(b). The sum of the direct and the exchange interaction gives

$$V(p'-p)-V(-p'-p)=2V(\sin p_x'\sin p_x+\sin p_y'\sin p_y)\ , \tag{20}$$

and we have, for this separable interaction,

$$t(p',p)=t_x \sin p_x' \sin p_x + t_y \sin p_y' \sin p_y \ , \tag{21}$$

with

$$t_x=t_y=\frac{2V}{1+(V/N)\sum_p (\sin^2 p_x+\sin^2 p_y)[1-2f(\epsilon_p)/2\epsilon_p]} \ . \tag{22}$$

In this same approximation, the pairing susceptibility, Eq. (9), can be written as

$$P(q)=\frac{P_0(q)}{1+2VP_0(q)} \ , \tag{23}$$

with

$$P_0(q)=\sum_q \left[\sin^2\left[p_x+\frac{q_x}{2}\right]+\sin^2\left[p_y+\frac{q_y}{2}\right]\right] \times \frac{1-f(\epsilon_{p+q})-f(\epsilon_p)}{\epsilon_{p+q}+\epsilon_p} \ . \tag{24}$$

For $V<0$, both $P(0)$ and the t matrix has a pole at a temperature $T_{\rm TP}$ given by

$$1=\frac{|V|}{N}\sum_p (\sin^2 p_x+\sin^2 p_y)\frac{\tanh(\beta_{\rm TP}\epsilon_p/2)}{2\epsilon_p} \ . \tag{25}$$

At low temperatures, the average of $\sin^2 p_x+\sin^2 p_y$ over the Fermi surface of Fig. 2 gives 1, so that we can use the results of Eq. (17) to obtain the weak-coupling limit,

$$T_{\rm TP}\simeq 2\exp(-2\pi/\sqrt{|V|}) \ , \tag{26}$$

which eventually dominates over the condensation transition temperature equation (16). Solving for $T_{\rm TP}$ using the full expression given by Eq. (17) and equating it to $T_{\rm con}$, we find that $T_{\rm TP}$ exceeds $T_{\rm con}$ for $-0.38<V<0$.

To summarize, the weak-coupling limits of the RPA predict that for $V>0$ a transition to a $2p_F$ density wave will occur when

$$T_{\rm DW}\cong 2\exp(-\pi/\sqrt{V}) \ . \tag{27}$$

For $-0.38<V<0$ triplet pairing occurs at a higher transition temperature,

$$T_{\rm TP}\cong 2\exp(-2\pi/\sqrt{V}) \ , \tag{28}$$

than the condensation transition,

$$T_{\rm con}=16\exp(-\pi^2/2|V|) \ , \tag{29}$$

which is highest for $V<-0.38$.

It is also interesting to examine the strong-coupling limits of the RPA predictions. Since $T\propto V$, the strong-coupling limit is also the high-temperature limit. For example, when $q=2p_F$,

$$\Pi_0(2p_F)=\frac{1}{N}\sum_p \frac{\tanh(\beta\epsilon_p/2)}{2\epsilon_p} \ , \tag{30}$$

since $\epsilon_{p+2p_F}=-\epsilon_p$. Expanding the tanh, we find that

$$\Pi_0(2p_F)=\frac{\beta}{4}\left[1-\frac{\beta^2}{3}+\cdots\right] , \tag{31}$$

so that solving Eq. (18) for $T_{\rm DW}$ to leading order in t/V gives

$$T_{\rm DW}=V\left[1-\frac{1}{3}\left[\frac{t}{V}\right]^2+\cdots\right] . \tag{32}$$

Here we have put the hopping energy t in explicitly. Thus, as V decreases, the system deviates below the Weiss mean-field transition temperature $T_{\rm DW}=V$. In a similar manner, we find that

$$T_{\rm con}=|V|\left[1-\left[\frac{t}{V}\right]^2+\cdots\right] . \tag{33}$$

The RPA results for $T_{\rm DW}$ for $V>0$ and the weak- and strong-coupling approximations to the RPA are shown in Fig. 4. Figure 5 shows the same thing for $T_{\rm con}$ versus $-V$, and Fig. 6 shows the low-temperature crossover where $T_{\rm TP}$ exceeds $T_{\rm con}$.

The strong-coupling limits, Eqs. (32) and (33), of the RPA expression go to the mean-field $T=|V|$ result when $|V|/t\gg 1$. A true strong-coupling expansion would approach the known Ising result $T=0.56|V|$ in this limit. In principle, the procedure for constructing a strong-coupling expansion is straightforward. For example, expanding Z in powers of the hopping term t, we have

$$Z=\mathrm{Tr}\left[e^{-\beta H_I}\left[1+\int_0^\beta d\tau_1\int_0^{\tau_1}d\tau_2\,T(\tau_1)T(\tau_2)+\int_0^\beta d\tau_1\int_0^{\tau_1}d\tau_2\int_0^{\tau_2}d\tau_3\int_0^{\tau_3}d\tau_4\,T(\tau_1)T(\tau_2)T(\tau_3)T(\tau_4)+\cdots\right]\right] . \tag{34}$$

Here $T(\tau)$ is given by

$$T(\tau)=e^{H_I\tau}\left[\sum_{\langle ij\rangle}-t(c_i^\dagger c_j+c_j^\dagger c_i)\right]e^{-H_I T} \ , \tag{35}$$

and H_I is the near-neighbor interaction [second term in Eq. (1)]. The terms containing odd powers of T vanish. High-temperature-series expansion techniques can be used to evaluate these terms in powers of $\tanh(\beta V)$, and a Padé approximation constructed for the specific heat or a relevant susceptibility. From this type of analysis the effect of $(t/V)^2$ on $T_{\rm con}$ and $T_{\rm DW}$ as well as estimates for the indices of the transition could be obtained.

Clearly, such an analysis would be a major project, but to leading order in $(t/V)^2$ the effect of $c_i^\dagger c_j$ operators in the kinetic-energy terms can be duplicated by the spin-$\frac{1}{2}$

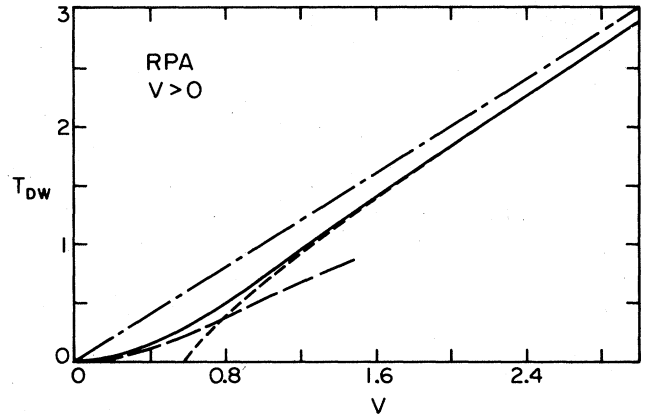

FIG. 4. Solid curves give the RPA result for T_{DW} versus V. Short-dashed curve is the strong-coupling limit, Eq. (32), and the long-dashed line is obtained from Eq. (18) using the low-temperature expansion of Π_0, Eq. (17). The long-dashed–short-dashed curve is the Weiss mean-field result $T_{DW}=V$.

operators $S_i^+S_j^-$. This follows since with two factors of T, see Eq. (34), a fermion can only go to a site and then return. Two fermions cannot exchange until order $(t/V)^4$, so that the kinetic fermion sign factors are not present to order $(t/V)^2$. With the replacement of the fermion $c_i^\dagger c_j$ operators by the spin operators $S_i^+S_j^-$ and $(n_i-\frac{1}{2})(n_j-\frac{1}{2})$ by $S_i^zS_j^z$, the problem reduces to finding the initial suppression of the Ising transition temperature for an anisotropic, $J_x/J_z \ll 1$, two-dimensional Heisenberg-Ising model. Here a number of authors[12] have carried out high-temperature-series expansions for the ferromagnetic case to obtain the transition temperature and the indices characteristic of the transitions. They conclude that the indices are those of the 2D Ising model until $J_x=J_z$, where the transition temperature goes to zero for the spin problem. Fitting their results for the transition temperature as shown in Fig. 7, we find, to leading order in $(t/V)^2$,

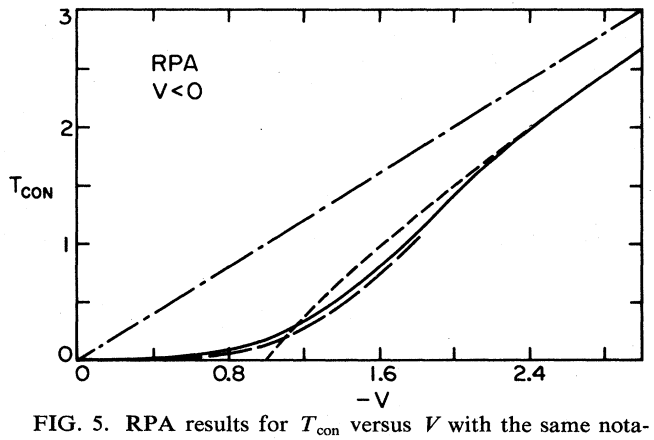

FIG. 5. RPA results for T_{con} versus V with the same notation as Fig. 4. The short-dashed strong-coupling curve is obtained from Eq. (33) and the long-dashed curve from Eq. (16).

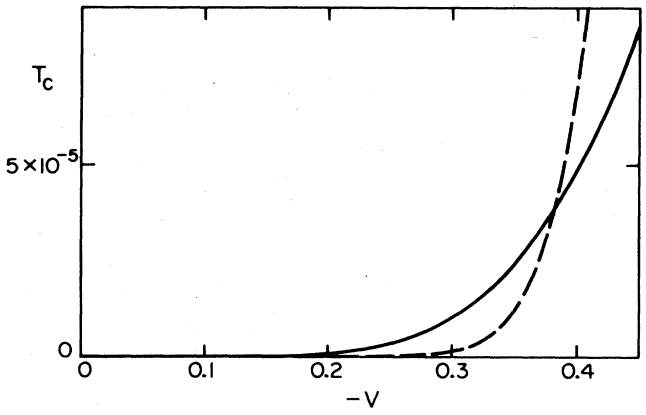

FIG. 6. Weak-coupling low-temperature regime in which the t matrix or pairing susceptibility $P(0)$ (solid line) diverges at a higher temperature than the condensation transition (dashed line).

$$T_{con} \cong 0.56V[1-(t/V)^2] \,. \tag{36}$$

This is similar to the RPA result except for the factor of 0.56.

III. MONTE CARLO SIMULATIONS

Using the fermion Monte Carlo method described in the Appendix, we have carried out numerical simulations for both positive and negative values of V. As discussed in the Appendix, each updating of a lattice variable requires N^2 operations, where N is the total number of lattice sites. Therefore, to perform an updating of all the variables in a two-dimensional $N=L\times L$ system requires $L^6\times M$ operations, where M is the number of time slices. This restricts the size of the lattices that can be studied, and the work reported here is based upon lattices with $L \leq 12$. In order to infer the characteristics of a macroscopic system from lattices of this size, we will make use of the ideas of finite-size scaling.

Using the techniques described in the Appendix, it is straightforward to evaluate finite-temperature single-particle Green's functions as well as a variety of particle-hole and two-particle response functions which provide information on the quantum correlations in the system.

For example, we have evaluated the Fourier transform of the equal-time single-particle Green's function to obtain the momentum occupation number,

$$\langle n_p \rangle = \frac{1}{N}\sum_{l,m} e^{ip\cdot(l-m)}\langle c_m^\dagger c_l \rangle \,. \tag{37}$$

For $V=0$, this is, of course, just the usual Fermi function

$$f(\epsilon_p)=[\exp(\beta\epsilon_p)+1]^{-1}$$

with ϵ_p the band energy, Eq. (5). However, as illustrated in Figs. 8(a) and 8(b), $\langle n_p \rangle$ for the interacting system can show significant deviations from $f(\epsilon_p)$. We will return later to a discussion of these results.

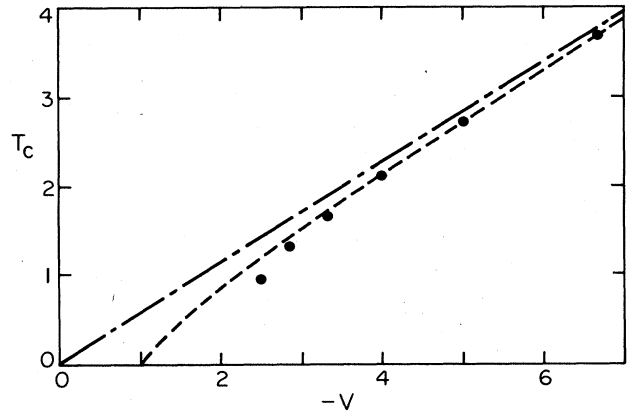

FIG. 7. Dots show the results for T_{con} obtained from a high-temperature-series expansion of the anisotropic Heisenberg-Ising model, Ref. 2. The dashed curve is a fit to the large $|V|$ part of this data, Eq. (36). The long-dashed–short-dashed line is the Kramers-Wannier Ising-model result $T_c=0.56|V|$.

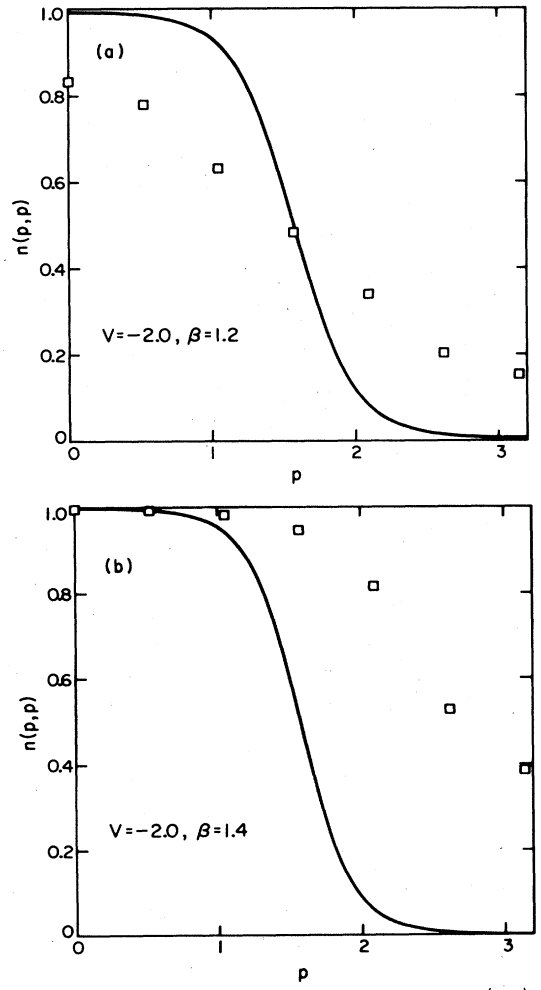

FIG. 8. Fermion momentum occupation number $\langle n_p \rangle$ versus momentum $\mathbf{p}=(p,p)$ for $V=-2.0$, and (a) $\beta=1.2$ (above the condensation transition) and (b) $\beta=1.4$ (below the condensation transition).

The nature of the density-density correlations are often analyzed in terms of the structure factor

$$S(q)=\frac{1}{N}\sum_{l,m} e^{iq\cdot(l-m)}\langle (n_l-\tfrac{1}{2})(n_m-\tfrac{1}{2})\rangle \ . \tag{38}$$

Figure 9 shows $S(q)$ at various temperatures obtained from our numerical simulations on 12×12 lattices for $V=-2$. As previously discussed, for negative values of V the system can undergo a condensation transition, giving rise to a peak in $S(q)$ at $q=(0,0)$, or possibly exhibit a tendency towards odd angular-momentum pairing. For $V=-2$, $S(q)$ in Fig. 9 shows the development of a large condensation peak at $q=0$.

In order to extrapolate to the bulk limit, we have carried out simulations on different sized lattices. Figure 10 shows how the peak $S(0,0)$ for $V=-2$ varies with temperature for lattices with $L=4$, 6, 8, 10, and 12. The height of the peak at low temperature is proportional to the lattice size, while at high temperatures its value is independent of L. Near the transition temperature T_{con} of the bulk system, correlations associated with a second-order transition in a 2D lattice fall off as $r^{-\eta}\exp(-r/\xi)$, with $\xi\sim|\beta-\beta_c|^{-\nu}$. Thus, for a lattice of size L we have

$$S(0,0)\sim L^{2-\eta}f(L^{1/\nu}(\beta-\beta_c)) \ . \tag{39}$$

For $V\gg t$, our model goes over to the 2D Ising antiferromagnetic model. As V/t decreases from positive values, the transition temperature T_{DW} moves continuously from the Ising limit. As previously discussed, an expansion in the hopping introduces only finite-range effective spin couplings, so that for weak hopping the system remains in the 2D Ising universality class. This same type of analogy to the ferromagnetic Ising model holds for the condensation transition when $V<0$ and $|V|\gg t$. Naturally, as t increases so that $t\gtrsim|V|$, it is possible to have a crossover to other types of fixed points, such as, for example, an XY fixed point for the triplet-pairing phase. However, within the parameter range presently accessible to our simulations, we have found only density-wave ($V>0$) and condensation ($V<0$) transitions. Therefore, we have analyzed our results for $S(0,0)$ and $S(\pi,\pi)$ using the 2D Ising indices $\eta=\frac{1}{4}$ and $\nu=1$.

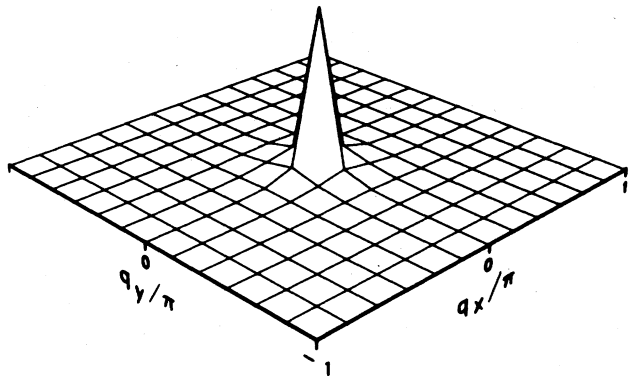

FIG. 9. Structure factor $S(q)$ versus q for $V=-2.0$ at a value of $\beta=1.2$. The long-wavelength density fluctuations give rise to the peak at $q=0$.

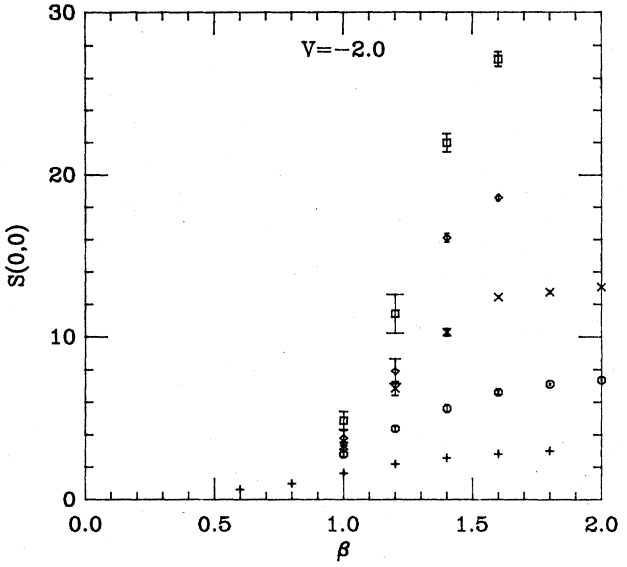

FIG. 10. $S(0,0)$ versus β for various sized lattices with $V=-2$. In this and all similar figures, the error bars marked with plus signs represent 4×4 lattices, the octagons 6×6 lattices, the diagonal crosses 8×8 lattices, the diamonds 10×10 lattices, and the squares 12×12 lattices.

In Fig. 11 we have replotted the data of Fig. 10 in terms of the scaled quantities $S(0,0)/L^{7/4}$ and tL with $t=(\beta-\beta_c)/\beta_c$ and $\beta_c=1.3$. Empirically, using $(\beta-\beta_c)/\beta_c$ gave finite-size scaling over a larger range than $(T-T_c)/T_c$. Naturally, the degree of superposition of the data from lattices of different sizes depends upon the choice of β_c and, in fact, provides a way of estimating β_c. We will examine this in more detail for the absolute value of the order parameter.

For $V>0$, the density-wave transition can be characterized by an order parameter O_{DW} with

$$|O_{\mathrm{DW}}|=\left\langle\left|\frac{1}{N}\sum_l(-1)^{l_x+l_y}(n_l-\tfrac{1}{2})\right|\right\rangle, \tag{40}$$

while for $V<0$ the condensation transition has

$$|O_{\mathrm{con}}|=\left\langle\left|\frac{1}{N}\sum_l(n_l-\tfrac{1}{2})\right|\right\rangle. \tag{41}$$

The normalization is such that $\langle|O|\rangle$ ranges from 0 to 0.5. On a finite lattice, the expectation value of the order parameter in the limit of a sufficiently long Monte Carlo run is equal to zero even in the temperature regime corresponding to an ordered phase of the bulk system. For this reason we have evaluated the absolute values of the order parameter, Eqs. (40) and (41), respectively. In the high-temperature phase, there will be a number of independent domains proportional to the area of the system so that with our normalization $\langle|O|\rangle$ will vary as $N^{-1/2}$. For T near T_c, the bulk order parameter varies as $(T-T_c)^{\beta}$ and, using the Ising value of $\beta=\frac{1}{8}$, finite-size scaling predicts that

$$\langle|O|\rangle\sim L^{1/8}F((\beta-\beta_c)L). \tag{42}$$

The absolute value of the order parameter,

$$\langle|O_{\mathrm{Ising}}|\rangle=\left\langle\left|\frac{1}{N}\sum_i S_i^z\right|\right\rangle, \tag{43}$$

for the 2D Ising model ($V\to\infty$), measured on lattices of several different sizes, is shown in Fig. 12. In this case we know $\beta_c=0.44$ and Fig. 13 shows the scaled order parameter $\langle|O_{\mathrm{Ising}}|\rangle L^{1/8}$ plotted versus tL with $t=(\beta-\beta_c)/\beta_c$.

Returning to the quantum problem, Fig. 14 shows $\langle|O_{\mathrm{con}}|\rangle$ versus β for $V=-2$ and various sized lattices. Using the finite-size scaling relation (42), we have replotted this data in Fig. 15 for three different values of β_c. Based upon these results and similar ones for $S(0,0)$, we

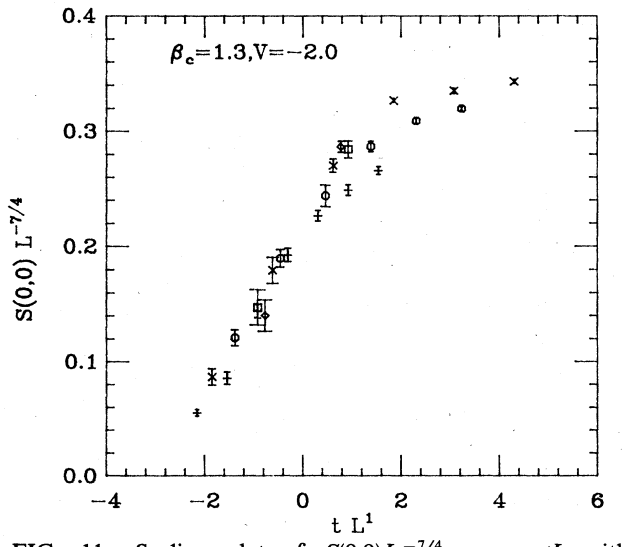

FIG. 11. Scaling plot of $S(0,0)L^{-7/4}$ versus tL with $t=(\beta-\beta_c)/\beta_c$ and $\beta_c=1.3$. Here, $V=-2$.

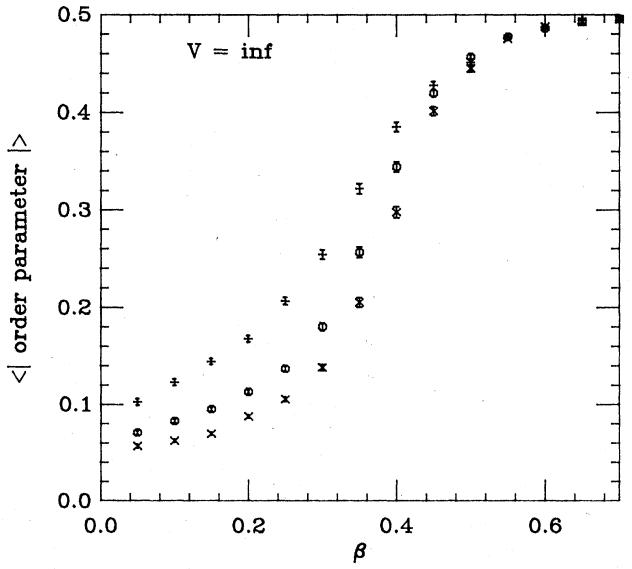

FIG. 12. Absolute value of the Ising order parameter $\langle|O_{\mathrm{Ising}}|\rangle$ versus β for various sized lattices.

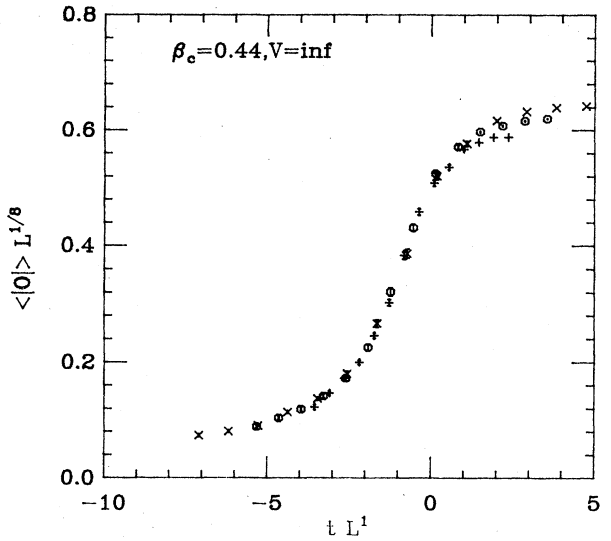

FIG. 13. Scaled Ising order parameter $\langle\,|\,O_{\rm Ising}\,|\,\rangle L^{1/8}$ versus tL using the data of Fig. 14 with $\beta_c=0.44$.

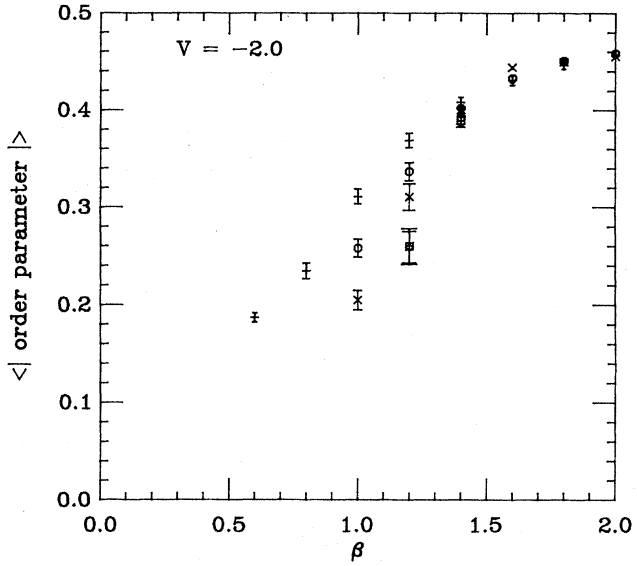

FIG. 14. $\langle\,|\,O_{\rm con}\,|\,\rangle$ versus β for $V=-2$ and various sized lattices.

believe that $\beta_{\rm con}=1.30\pm0.07$ for $V=-2$.

We have prepared similar graphs for all the simulated values of V, both positive and negative. Estimates of $\beta_{\rm con}$ and $\beta_{\rm DW}$ were made by estimating the value of β for which the scaled data were best superimposed. Results for the transition temperatures for different values of V are summarized in Table I. Notice that $T_{\rm con}$ is lower than $T_{\rm DW}$ for the same magnitude of V. This can be understood as a consequence of the "Fermi hole," or the fact that even for $V=0$ the density-density correlation is suppressed at short distances. For $V<0$ the interaction must compete with the Fermi repulsion. Therefore, larger values of V, or lower temperatures, are required for the condensation transition than for the density-wave transition.

To illustrate the Ising character of these transitions, Fig. 16 shows scaled results for the absolute value of the order parameter for different values of V. It also contains the data for the classical 2D Ising model. In this figure the value of the abscissa has been translated by an arbitrary amount to separate the different curves.

It is also interesting to examine the distribution of values of the order parameter,

$$\langle O_{\rm con}\rangle=\left\langle\frac{1}{N}\sum_l(n_l-\tfrac{1}{2})\right\rangle . \tag{44}$$

As we previously noted, the average value of the order parameter vanishes for a finite system. However, the distribution of $\langle O_{\rm con}\rangle$ values obtained in Monte Carlo runs at different temperatures are plotted in Fig. 17 and clearly show a condensation transition. On the high-temperature side of the transition, the distribution of $\langle O_{\rm con}\rangle$ forms a single peak about $\langle n\rangle=0.5$, while at low temperature, two distinct peaks with $\langle n_1\rangle\simeq0.9$ and $\langle n_2\rangle\simeq0.1$ are evident. At low temperatures it is possible for a Monte Carlo run on a large lattice (12×12) to simply remain frozen in one of these two states. This is what happened in the run where $\langle n_p\rangle$, Fig. 8(b), was measured, and explains why $\sum_p\langle n_p\rangle=0.889$ rather than 0.5.

We have also calculated the zero-frequency density-density susceptibility

$$\Pi(q)=\frac{1}{N}\sum_{l,m}e^{iq\cdot(l-m)}\int_0^\beta\langle n_l(\tau)n_m(0)\rangle d\tau . \tag{45}$$

For $q=(\pi,\pi)$ this gives the staggered susceptibility, whose divergence signals the onset of the density-wave transition for $V>0$. For $V<0$, $\Pi(0)$ is equal to the compressibility, which diverges at the condensation transition. Following the same arguments as previously used, we expect these quantities to scale like the susceptibility of the 2D Ising model with $\gamma=\frac{7}{4}$:

$$\Pi(t,L)=L^{7/4}f((\beta-\beta_c)L) . \tag{46}$$

Results for $\Pi(\pi,\pi)$ for $V=1$ are shown in Fig. 18 with the corresponding scaling plots given in Fig. 19. For $V<0$, $\Pi(0)$ is plagued by large statistical errors and gives us no useful information.

The excellent superposition of data from different sized lattices for S, $\langle\,|\,O\,|\,\rangle$, and $\Pi(\pi,\pi)$ using scaling based upon the 2D Ising indices and the close similarity of the results to the 2D Ising model lends numerical support to

TABLE I. Monte Carlo estimates of critical temperatures. For $V>0$ this is $T_{\rm DW}$, and for $V<0$ it is $T_{\rm con}$.

V	β_c	T_c	$\frac{T_c}{T_{\rm Ising}}$
0.75	>3.5	<0.29	<0.68
1.0	2.4±0.2	0.42±0.04	0.75±0.06
1.5	1.4±0.1	0.71±0.05	0.85±0.06
2.0	0.9±0.1	1.11±0.12	0.98±0.09
−1.75	2.0 ±0.3	0.50±0.08	0.51±0.08
−2.0	1.30±0.07	0.77±0.04	0.69±0.04
−2.5	0.85±0.05	1.18±0.07	0.84±0.05

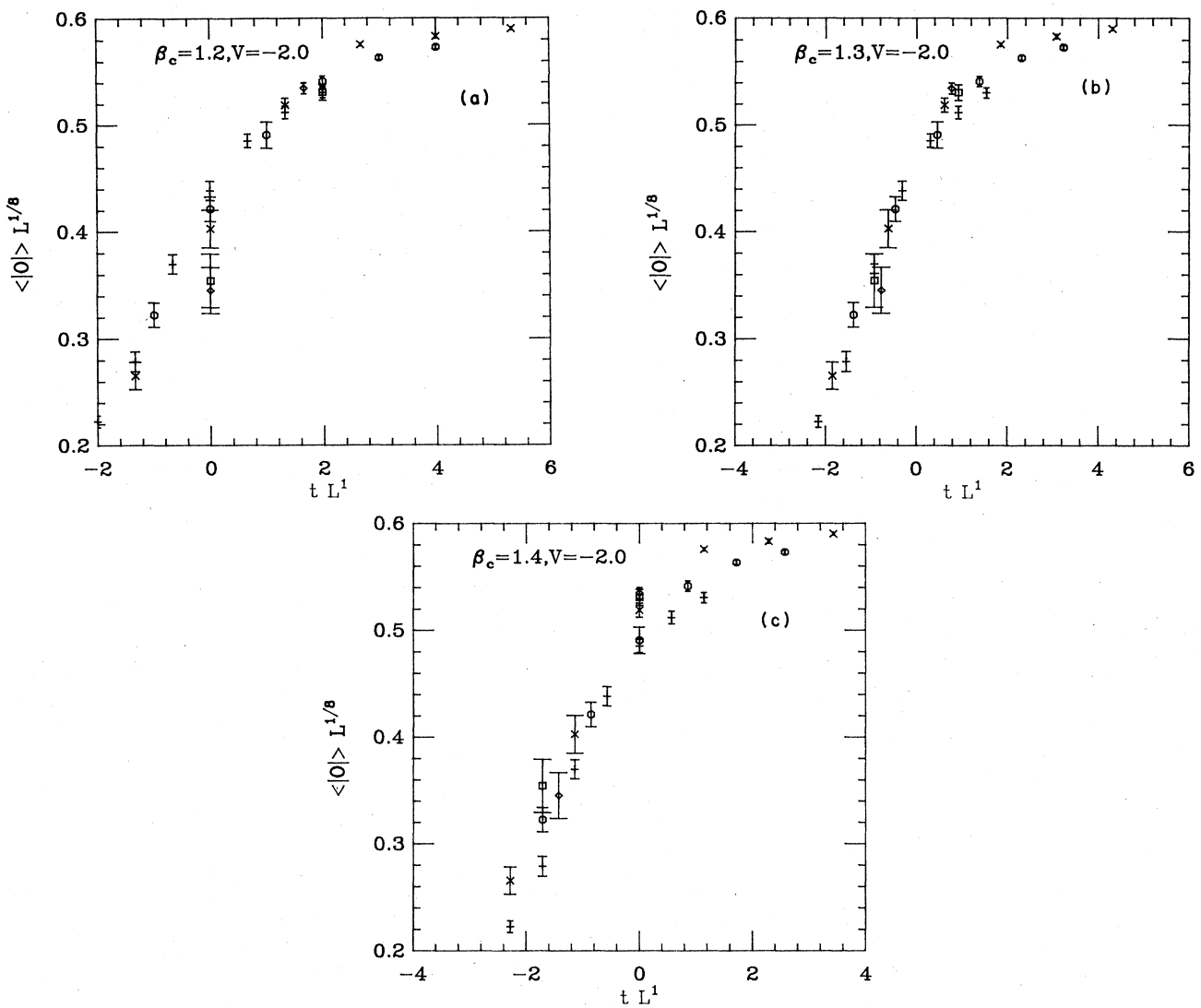

FIG. 15. Scaled data from Fig. 14, $\langle \mid O_{\rm con} \mid \rangle L^{1/8}$ versus tL with $t=(\beta-\beta_c)/\beta_c$ for (a) $\beta_c=1.2$, (b) $\beta_c=1.3$, and (c) $\beta_c=1.4$.

our arguments that the density-wave ($V>0$) and condensation ($V<0$) transitions are indeed in the Ising universality class. Unfortunately, at present, we have not been able to extend these simulations to the low-temperature, small-(V/t) regime. As explained in the Appendix, our Monte Carlo algorithm becomes inefficient at very low temperatures. Thus we have not been able to determine numerically whether the phase boundary for the density-wave transition extends into the origin, as suggested by the RPA result, or goes to $T_c=0$ at a finite value of V.[13] Likewise, for small negative values of V we do not know if an odd angular-momentum-pairing phase is present. We do see an increase pairing susceptibility $P(0)$ as the temperature is lowered for small negative values of V. However, $\Pi(0)$ is also increasing, and the simulations are not able to provide sufficient information to determine the low-temperature phase.

IV. CONCLUSION

The problem of a two-dimensional spin-polarized fermion half-filled lattice gas interacting through a near-neighbor coupling has been investigated. Our results and conclusions can be simply illustrated by the phase diagram shown in Fig. 20. The long-dashed—short-dashed line represents the classical Ising result, appropriate for $V/t\rightarrow\infty$. The dashed line represents the strong-coupling $\mid V \mid /t \gg 1$ solution for the condensation transition equation (3) for negative values of V. For positive values of V

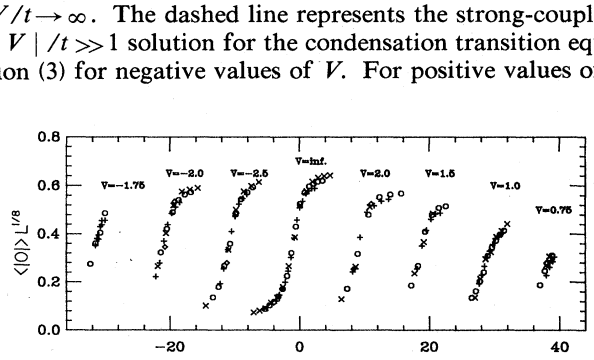

FIG. 16. Scaled results for the order parameter $\langle \mid O \mid \rangle L^{1/8}$ versus tL for different values of V. The abscissa has been translated by an arbitrary amount to separate the different curves.

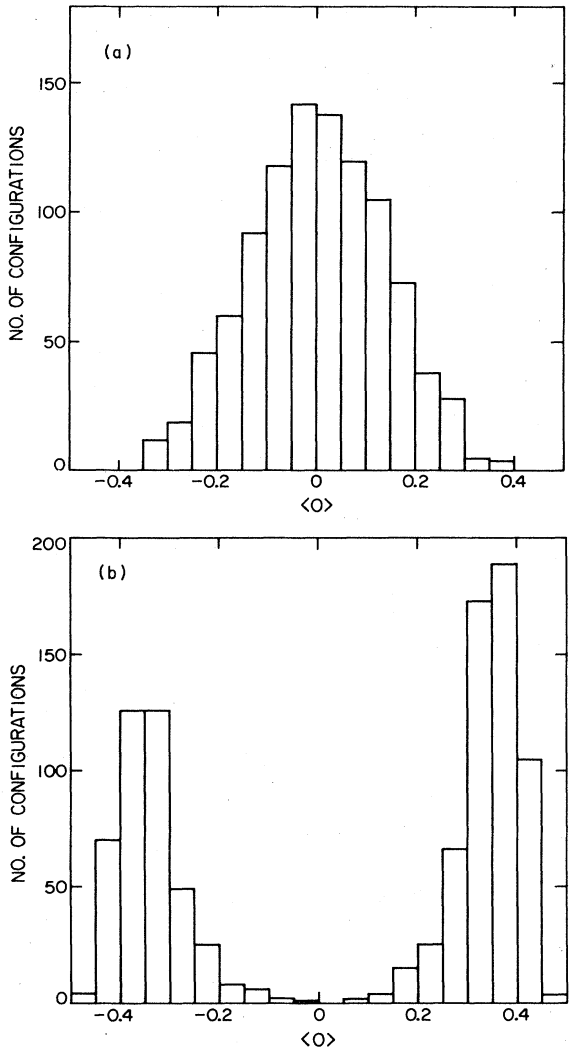

FIG. 17. Distribution of $\langle O_{\rm con} \rangle$ values on a 6×6 lattice for (a) a value of β above the transition, and (b) a value of β below the transition.

we were unable to find high-temperature-series expansions for the antiferromagnetic Heisenberg-Ising model, so we have simply taken the RPA coefficient of $\frac{1}{3}$ from Eq. (32) and plotted

$$T_{\rm DW}=0.56V[1-\tfrac{1}{3}(t/V)^2]\ . \tag{47}$$

The points with error bars represent the results for the condensation transition from our Monte Carlo simulations. A weak-coupling theory is needed to complete the phase diagram. As discussed in Sec. II, RPA-like calculations suggest that at small negative values of V/t and low temperatures an odd angular-momentum-pairing phase exists. If indeed this is the case, it is likely to be an XY-like phase with only topological order. Such a phase poses real difficulties for numerical simulations, again emphasizing the importance of developing a weak-coupling theory.

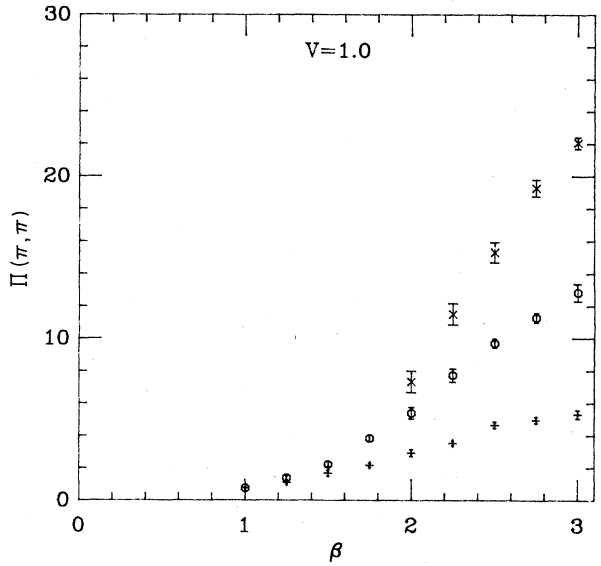

FIG. 18. Staggered susceptibility $\Pi(\pi,\pi)$ versus β for $V=1$ and various sized lattices.

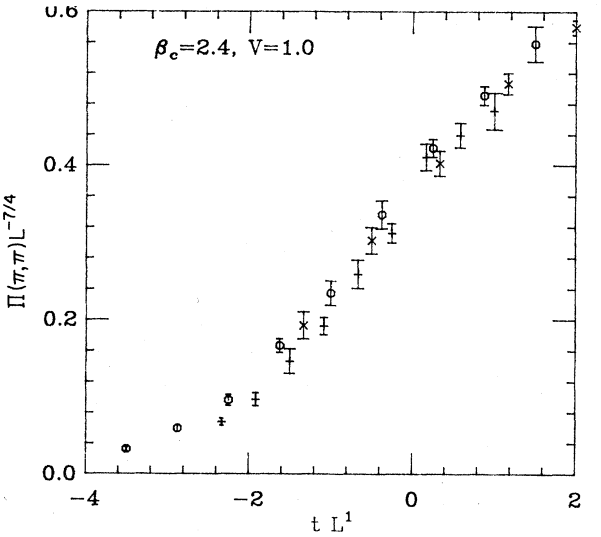

FIG. 19. Scaled plot of the data of Fig. 18, $\Pi(\pi,\pi)L^{-7/4}$ versus tL with $\beta_c=2.4$.

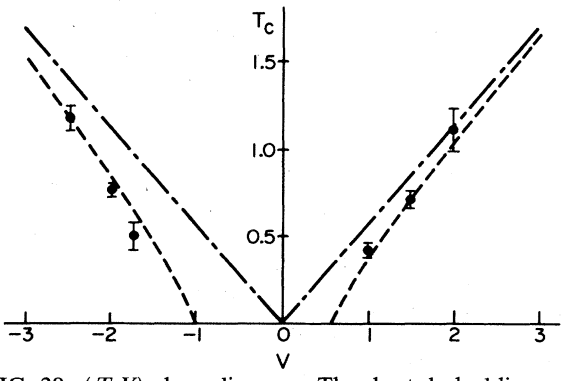

FIG. 20. (T,V) phase diagram. The short-dashed line corresponds to the Ising result $T_c=0.56\,|\,V\,|$. The dashed line is the strong-coupling limit, and the dots with error bars are obtained from the finite-size scaling analysis of the Monte Carlo data.

ACKNOWLEDGMENTS

We thank Gloria Buendia for providing the classical Ising data and Richard Scalettar for helping with the strong-coupling analysis. This work was supported in part by U.S. Department of Energy Contracts No. W-7405-Eng-36, No. DE-AT03-83ER45008, and No. DE-AT03-81ER40029, and National Science Foundation Grants No. PHY-80-18939 and No. PHY-77-27084 supplemented by funds from the U.S. National Aeronautics and Space Administration. We gratefully acknowledge E. I. du Pont de Nemours and Company and the Xerox Corporation for their support.

APPENDIX

In this appendix we discuss some details of the Monte Carlo calculation based on the general approach presented in Ref. 2.

We are interested in calculating correlation functions of the form

$$\langle T[A(\tau)B(\tau')]\rangle = \mathrm{tr}\{e^{-\beta H}T[A(\tau)B(\tau')]\}/\mathrm{tr}\, e^{-\beta H}\ , \tag{A1}$$

where

$$A(\tau)=e^{\tau H}A\, e^{-\tau H}\ ,$$
$$B(\tau')=e^{\tau' H}B\, e^{-\tau' H}\ . \tag{A2}$$

A and B are functions of the creation and annihilation operators $c_i^\dagger, c_i$ defined in Eq. (2) and $0\le\tau,\ \tau'<\beta$. H is the Hamiltonian of Eq. (1).

In order to construct an expression which can be evaluated with an importance-sampling Monte Carlo algorithm, we first perform the traces over the fermion degrees of freedom. The initial step in this process is to divide the interval 0 to β into M subintervals of width $\Delta\tau$ so $\beta=\Delta\tau M$. We restrict the values of τ and τ' to $\tau_l=l\,\Delta\tau$ with $l=0,1,2,\ldots,M-1$. The point $\tau_M=\beta=M\,\Delta\tau$ is identified with $\tau_0=0$.

The operator which translates the system through the lth imaginary-time interval, that is from τ_{l-1} to τ_l, will be denoted by U_l,

$$U_l=e^{-\Delta\tau H}\ . \tag{A3}$$

Then, using the fact that $\Delta\tau$ times the characteristic energies in H are small, we approximate U_l by

$$U_l\simeq e^{-\Delta\tau H_0}e^{-\Delta\tau H_I}\ . \tag{A4}$$

Here,

$$H=H_0+H_I\ , \tag{A5}$$

with

$$H_0=-t\sum_{\langle ij\rangle}(c_i^\dagger c_j+c_j^\dagger c_i) \tag{A6}$$

and

$$H_I=V\sum_{\langle ij\rangle}(n_i-\tfrac{1}{2})(n_j-\tfrac{1}{2})\ . \tag{A7}$$

The term $\exp(-\Delta\tau H_I)$ is then treated by making use of a discrete Hubbard-Stratonovich transformation introduced by Hirsch.[14] For $V>0$,

$$\exp[-\Delta\tau V(n_i-\tfrac{1}{2})(n_j-\tfrac{1}{2})]=\frac{e^{-\Delta\tau V/4}}{2}\sum_{S_{ij}(l)=\pm1}\exp[-\Delta\tau JS_{ij}(l)(n_i-n_j)]\ , \tag{A8}$$

with $\cosh(\Delta\tau J)=e^{\Delta\tau V/2}$, while for $V<0$,

$$\exp[-\Delta\tau V(n_i-\tfrac{1}{2})(n_j-\tfrac{1}{2})]=\frac{e^{\Delta\tau V/4}}{2}\sum_{S_{ij}(l)=\pm1}\exp[-\Delta\tau JS_{ij}(l)(n_i+n_j-1)]\ , \tag{A9}$$

with $\cosh(\Delta\tau J)=\exp(-\Delta\tau V/2)$. Note that $S_{ij}(l)$ is defined on the link between nearest-neighbor lattice points i and j, and in the interval between allowed imaginary times τ_{l-1} and τ_l.

Making use of Eqs. (A8) and (A9) and undoing the factorization of Eq. (A7), we can write

$$U_l=(\tfrac{1}{2}e^{-\Delta\tau|V|/4})^{2N}\sum_{\{S_{ij}(l)\}=\pm1}e^{-\Delta\tau H(l)}=\sum_{\{S_{ij}(l)\}=\pm1}u_l\ . \tag{A10}$$

N is the number of lattice sites. For $V>0$,

$$H(l)=\sum_{i,j}c_i^\dagger h_{ij}(l)c_j=-t\sum_{\langle ij\rangle}(c_i^\dagger c_j+c_j^\dagger c_i)+J\sum_i c_i^\dagger c_i\{[S_{i,i+\hat{x}}(l)-S_{i-\hat{x},i}(l)]+[S_{i,i+\hat{y}}(l)-S_{i-\hat{y},i}(l)]\}\ , \tag{A11}$$

while for $V<0$,

$$\begin{aligned}H(l)&=-J\sum_{\langle ij\rangle}S_{ij}(l)+\sum_{i,j}c_i^\dagger h_{ij}(l)c_j\\&=-J\sum_{\langle ij\rangle}S_{ij}(l)-t\sum_{\langle ij\rangle}(c_i^\dagger c_j+c_j^\dagger c_i)+J\sum_i c_i^\dagger c_i[S_{i,i+\hat{x}}(l)+S_{i-\hat{x},i}(l)+S_{i,i+\hat{y}}(l)+S_{i-\hat{y},i}(l)]\ .\end{aligned} \tag{A12}$$

Because $H(l)$ is quadratic in the fermion creation and annihilation operators, the traces over fermion coordinates can be evaluated in closed form. In effect, we have transformed the original problem into the problem of a system of fermions that have no self-interactions, but which are coupled to a fixed, imaginary-time-dependent spin field, $\{S_{ij}(l)\}$, which is summed over all possible configurations. This sum will be carried out using the Monte Carlo technique dis-

cussed in Ref. 3.

Let us start by considering the single-particle Green's function. Making use of Eqs. (A1)—(A3) and (A10), we write

$$G_{ij}(\tau_l,\tau_m)=\langle T[c_i(\tau_l)c_j^\dagger(\tau_m)]\rangle=\sum_{\{S\}} z g_{ij}(\tau_l,\tau_m)\Big/\sum_{\{S\}} z \ , \tag{A13}$$

where

$$z=\mathrm{tr}(u_M u_{M-1}\cdots u_2 u_1) \ . \tag{A14}$$

For $l\geq m$,

$$g_{ij}(\tau_l,\tau_m)=z^{-1}\mathrm{tr}(u_M u_{M-1}\cdots u_{l+1}c_i u_l\cdots u_{m+1}c_j^\dagger u_m\cdots u_1) \ , \tag{A15}$$

while for $l<m$,

$$g_{ij}(\tau_l,\tau_m)=-z^{-1}\mathrm{tr}[u_M u_{M-1}\cdots u_{m+1}c_j^\dagger u_m\cdots u_{l+1}c_i u_l\cdots u_1] \ . \tag{A16}$$

The sums in Eq. (A13) are over all spin configurations on all time intervals.

$g_{ij}(\tau_l,\tau_m)$ is obviously the single-particle Green's function for a fermion in a fixed, time-dependent external spin field. Making use of the identity

$$c_i u_l=u_l(e^{-\Delta\tau\underline{h}(l)})_{ij}c_j\equiv u_l(B_l)_{ij}c_j \ , \tag{A17}$$

which follows directly from Eqs. (2) and (A10)—(A12), we see that, for $l\neq 0$,

$$g_{ij}(\tau_l,\tau_m)=(B_l)_{ik}g_{kj}(\tau_{l-1},\tau_m) \tag{A18}$$

and

$$g_{ij}(\tau_0,\tau_m)=-(B_M)_{ik}g_{kj}(\tau_{M-1},\tau_m) \ . \tag{A19}$$

Summation over repeated indices is implied.

Iterating Eqs. (A18) and (A19) M times and making use of Eq. (2), we find that

$$(\underline{I}+\underline{B}_m\underline{B}_{m-1}\cdots\underline{B}_2\underline{B}_1\underline{B}_M\underline{B}_{M-1}\cdots\underline{B}_{m+2}\underline{B}_{m+1})_{ik}g_k(\tau_m,\tau_m)\equiv F_{ik}(m)g_{kj}(\tau_m,\tau_m)=\delta_{ij} \ . \tag{A20}$$

$\underline{I}$ is the unit matrix, $I_{ik}=\delta_{ik}$. Adopting matrix notation for g, we see that

$$\begin{aligned}
&\underline{g}(\tau_m,\tau_m)=[\underline{F}(m)]^{-1} \ , \\
&\underline{g}(\tau_l,\tau_m)=\underline{B}_l\underline{B}_{l-1}\cdots\underline{B}_{m+1}\underline{F}^{-1}(m), \quad l>m \\
&\underline{g}(\tau_l,\tau_m)=-\underline{B}_l\underline{B}_{l-1}\cdots\underline{B}_2\underline{B}_1\underline{B}_M\underline{B}_{M-1}\cdots\underline{B}_{m+1}\underline{F}^{-1}(m), \quad l<m \ .
\end{aligned} \tag{A21}$$

The next step is to calculate the spin-dependent partition function z. We assert that

$$z=\det(\underline{I}+\underline{B}_M\underline{B}_{M-1}\cdots\underline{B}_2\underline{B}_1), \quad V>0 \tag{A22}$$

and

$$z=e^{\Delta\tau J}\sum_{l,\langle ij\rangle} S_{ij}(l)\det(\underline{I}+\underline{B}_M\underline{B}_{M-1}\cdots\underline{B}_2\underline{B}_1) \ , V<0 \tag{A23}$$

where we have dropped the trivial factors $(\frac{1}{2}e^{-\Delta\tau}\,|\,V\,|\,/2)^{2N}$ of Eq. (A10) since they do not enter into any physical results.

Let us begin with Eq. (A22). We first note that it is correct for $\Delta\tau=0$. Next we see from Eqs. (A10)—(A12) and (A21) that

$$\frac{d}{d\,\Delta\tau}\ln(z)=-\sum_{l=1}^{M-1}\mathrm{tr}\{[\underline{I}-\underline{g}(\tau_{l-1},\tau_{l-1})]\underline{h}(l)\} \ . \tag{A24}$$

Differentiating the logarithm of the right-hand side of Eq. (A22) gives the same result as can be seen from Eqs. (A17) and (A21). Integrating the derivatives from 0 to $\Delta\tau$ gives Eq. (A22). Equation (A23) follows from the same set of arguments.

We are also interested in correlation functions with four or more fermion creation and annihilation operators. Using the above reasoning, or simply making use of Wick's theorem, we find, for example, that

$$\begin{aligned}
G_{i_1i_2;j_1j_2}(\tau_{l_1},\tau_{l_2};\tau_{m_1},\tau_{m_2})&=\langle T[c_{i_1}(\tau_{l_1})c_{i_2}(\tau_{l_2})c_{j_2}^\dagger(\tau_{m_2})c_{j_1}^\dagger(\tau_{m_1})]\rangle \\
&=\sum_{\{S\}} z[g_{i_1j_1}(\tau_{l_1},\tau_{m_1})g_{i_2j_2}(\tau_{l_2},\tau_{m_2})-g_{i_1j_2}(\tau_{l_1},\tau_{m_2})g_{i_2j_1}(\tau_{l_2},\tau_{m_1})]\Big/\sum_{\{S\}} z \ .
\end{aligned} \tag{A25}$$

We perform the sums over spins in Eqs. (A13) and (A25) by a Monte Carlo calculation. We generate sets of spin configurations with probability proportional to z. z plays the same role as the exponential of the action in boson Monte Carlo calculations.

In obtaining the spin configurations we make use of the

heat-bath algorithm to bring each spin into equilibrium with its environment. In determining whether a particular spin should point up or down, we are required to calculate the ratio of the values of z for these two spin states. We now turn to the problem of evaluating this ratio.

It is convenient to express the single-particle Hamiltonian, $\underline{h}(l)$, defined in Eqs. (A11) and (A12) as a sum over link Hamiltonians. We denote two nearest-neighbor lattice points by $q=(q_x,q_y)$ and $p=(p_x,p_y)$ and write

$$\underline{h}(l)=\sum_{q,p}\underline{h}(q,p,l)\ . \tag{A26}$$

On an $L\times L$ spatial lattice the components of q and p can take on integer values ranging from 1 to L. In Eq. (A26) the sum is over all allowed values of q. For fixed q, p can take on the values (q_x+1,q_y) and (q_x,q_y+1) with the understanding that we are using periodic boundary conditions.

The $\underline{h}(q,p,l)$ are $L^2\times L^2$ matrices whose elements will be denoted by $h_{ij}(q,p,l)$, $i=(i_x,i_y)$, $j=(j_x,j_y)$. Referring to Eqs. (A11) and (A12), we see that only four of the elements are different from zero, and we can choose those to have the form

$$\begin{aligned}&h_{qq}(q,p,l)=JS_{qp}(l)\ ,\\ &h_{pp}(q,p,l)=\begin{cases}-JS_{qp}(l), & V>0\\ JS_{qp}(l), & V<0\end{cases}\\ &h_{qp}(q,p,l)=h_{pq}(q,p,l)=-t\ .\end{aligned} \tag{A27}$$

We shall refer to a link for which q_x is odd (even) and $p=(q_x+1,q_y)$ as an odd (even) x link, and a link for which q_y is odd (even) and $p=(q_x,q_y+1)$ as an odd (even) y link. We now rewrite Eq. (A26) in the form

$$\begin{aligned}\underline{h}(l)=&\sum_{\substack{\text{odd}\\ x\text{ links}}}\underline{h}(q,p,l)+\sum_{\substack{\text{even}\\ x\text{ links}}}\underline{h}(q,p,l)\\ &+\sum_{\substack{\text{odd}\\ y\text{ links}}}\underline{h}(q,p,l)+\sum_{\substack{\text{even}\\ y\text{ links}}}\underline{h}(q,p,l)\\ \equiv&\underline{h}^1(l)+\underline{h}^2(l)+\underline{h}^3(l)+\underline{h}^4(l)\ .\end{aligned} \tag{A28}$$

Each of the sub-Hamiltonians $h^s(l)$ is a sum of mutually commuting single-link Hamiltonians. Thus,

$$\underline{B}^1(l)=e^{-\Delta\tau\underline{h}^1(l)}=\prod_{\substack{\text{odd}\\ x\text{ links}}}\underline{B}(q,p,l)\ , \tag{A29}$$

with analogous expressions for the other sub-Hamiltonians. Here,

$$\underline{B}(q,p,l)=e^{-\Delta\tau\underline{h}(q,p,l)} \tag{A30}$$

is a symmetric $L^2\times L^2$ matrix with

$$\begin{aligned}&B_{ij}(q,p,l)=\delta_{ij},\quad i,j\neq q,p\\ &B_{iq}=B_{ip}=0,\quad i\neq q,p\ .\end{aligned} \tag{A31}$$

For $V>0$,

$$\begin{aligned}&B_{qq}(q,p,l)=\cosh(\Delta\tau\epsilon)-\frac{JS_{qp}(l)}{\epsilon}\sinh(\Delta\tau\epsilon)\ ,\\ &B_{pp}(q,p,l)=\cosh(\Delta\tau\epsilon)+\frac{JS_{qp}(l)}{\epsilon}\sinh(\Delta\tau\epsilon)\ ,\\ &B_{qp}(q,p,l)=B_{pq}(q,p,l)=\frac{t}{\epsilon}\sinh(\Delta\tau\epsilon)\ ,\end{aligned} \tag{A32}$$

with $\epsilon=(J^2+t^2)^{1/2}$, while, for $V<0$,

$$\begin{aligned}&B_{qq}(q,p,l)=B_{pp}(q,p,l)=e^{-\Delta\tau JS_{qp}(l)}\cosh(\Delta\tau t)\ ,\\ &B_{qp}(q,p,l)=B_{pq}(q,p,l)=e^{-\Delta\tau JS_{qp}(l)}\sin(\Delta\tau t)\ .\end{aligned} \tag{A33}$$

With errors of order $(\Delta\tau)^2$, we approximate $\underline{B}(k)$ by

$$\underline{B}(l)=\exp\left[-\Delta\tau\sum_{i=1}^{4}\underline{h}^i(l)\right]\simeq\underline{B}^4(l)\underline{B}^3(l)\underline{B}^2(l)\underline{B}^1(l)\ . \tag{A34}$$

Making use of this approximation, the determinant in the expressions for z becomes

$$\begin{aligned}D=&\det[\underline{I}+\underline{B}^4(M)\underline{B}^3(M)\underline{B}^2(M)\\ &\times\underline{B}^1(M)\underline{B}^4(M-1)\cdots\underline{B}^1(1)]\ .\end{aligned} \tag{A35}$$

From Eq. (A29) and analogous expressions for the other $\underline{B}^i(l)$, we see that D involves a very long ordered product of the $\underline{B}^i(q,p,l)$.

We are now in a position to calculate the change in D and hence z due to the flipping of a single spin, $S_{qp}(l)$. Since D is unchanged by a cyclic permutation of the $\underline{B}^i(l)$, we can assume that $\underline{B}(q,p,l)$ is the right most term in the product. That is, if $\underline{B}(q,p,l)$ is a factor in $\underline{B}^i(l)$, we write

$$D=\det[\underline{I}+\underline{B}^{i-1}(l)\cdots\underline{B}^1(l)\underline{B}^4(l-1)\cdots\underline{B}^1(l+1)\underline{B}^4(l)\cdots\underline{B}^i(l)]\equiv\det[\underline{I}+\underline{b}(l,i)]\ . \tag{A36}$$

Let us now imagine that $S_{qp}(l)\rightarrow -S_{qp}(l)$. Then,

$$\underline{B}(q,p,l)\rightarrow\underline{B}(q,p,l)[\underline{I}+\omega(q,p,l)]\ , \tag{A37}$$

where $\omega(q,p,l)$ is an $L^2\times L^2$ matrix which has only four nonzero elements, $\omega_{qq}(q,p,l)$, $\omega_{pp}(q,p,l)$, $\omega_{qp}(q,p,l)$, and $\omega_{qp}(q,p,l)$. Their values can be trivially computed from Eqs. (A32) and (A33).

We are interested in the ratio of the determinant after and before the spin flip,

$$\begin{aligned}R=&\det\{\underline{I}+\underline{b}(l,i)[\underline{I}+\underline{\omega}(q,p,l)]\}/\det[\underline{I}+\underline{b}(l,i)]\\ =&\det[\underline{I}+\underline{g}(l,i)\underline{b}(l,i)\underline{\omega}(q,p,l)]\\ =&\{1+[\underline{g}(l,i)\underline{b}(l,i)\underline{\omega}(q,p,l)]_{qq}\}\{1+[\underline{g}(l,i)\underline{b}(l,i)\underline{\omega}(q,p,l)]_{pp}\}-[\underline{g}(l,i)\underline{b}(l,i)\underline{\omega}(q,p,l)]_{qp}[\underline{g}(l,i)\underline{b}(l,i)\underline{\omega}(q,p,l)]_{pq}\ .\end{aligned} \tag{A38}$$

Here we have introduced

$$\underline{g}(l,i)=[\underline{I}+\underline{b}(l,i)]^{-1} . \tag{A39}$$

Notice that $\underline{g}(l,i)$ is just an extension of the single-particle equal-time Green's function. In fact, $\underline{g}(l,1)=g(\tau_{l-1},\tau_{l-1})$.

The numerical calculation of the ratio R is thus trivial; however, it does require a knowledge of the Green's function $\underline{g}(l,i)$. Suppose this matrix is stored in the computer and we do flip the spin $S_{qp}(l)$. We must then calculate the updated Green's function,

$$\begin{aligned}\underline{g}(l,i)\rightarrow\underline{g}_{f}(l,i)&\\ &=\{\underline{I}+\underline{b}(l,i)[\underline{I}+\underline{\omega}(q,p,l)]\}^{-1}\\ &=\underline{g}(l,i)-\underline{g}(l,i)\underline{b}(l,i)\underline{\omega}(q,p,l)\underline{g}_{f}(l,i) .\end{aligned} \tag{A40}$$

Because $\underline{\omega}(q,p,l)$ has only four nonzero elements, Eq. (A40) can be solved for $\underline{g}_{f}(l,i)$ merely by inverting a two-dimensional matrix. The bottleneck occurs because we must calculate all L^4 elements of $\underline{g}_{f}(l,i)$.

Once we have equilibrated each spin in $\underline{h}^{i}(l)$, we can go on to $\underline{h}^{i+1}(l)$, or $\underline{h}^{1}(l+1)$ if $i=4$, by making use of the relations

$$\begin{aligned}&\underline{g}(l,i+1)=\underline{B}^{i}(l)\underline{g}(l,i)[\underline{B}^{i}(l)]^{-1},\quad i=1,2,3\\ &\underline{g}(l+1,1)=\underline{B}^{4}(l)\underline{g}(l,4)[B^{4}(l)]^{-1} .\end{aligned} \tag{A41}$$

Because of the sparseness of the $\underline{B}^{i}(l)$, this calculation takes only of order L^4 numerical operations. Thus, if we calculate $g(1,1)$, for example, once at the beginning of the Monte Carlo process, we, in principle, never have to invert an $L^2\times L^2$ matrix again. We simply update the appropriate $\underline{g}(l,i)$ as we go along using Eqs. (A40) and (A41).

The one remaining problem is that roundoff errors accumulate in $\underline{g}(l,i)$; indeed, they are amplified by successive updates. Let us denote the difference between $\underline{g}(l,i)$ and the exact inverse of $\underline{I}+\underline{b}(l,i)$ by $\delta\underline{g}(l,i)$. Then,

$$\begin{aligned}\delta\underline{g}(l,i)=&\underline{g}(l,i)-\underline{g}(l,i)[\underline{I}+\underline{b}(l,i)]\underline{g}(l,i)\\ &+\delta\underline{g}(l,i)[\underline{I}+\underline{b}(l,i)]\delta\underline{g}(l,i) .\end{aligned} \tag{A42}$$

We drop the term on the right-hand side of Eq. (A42), which contains two factors of $\delta\underline{g}$, and thus obtain a simple first-order correction to $\underline{g}(l,i)$. We use this correction whenever roundoff errors cause us to lose approximately half the significant figures in the elements of $\underline{g}(l,i)$. Full machine accuracy is generally restored. The frequency with which one must make this correction is strongly dependent on β and the other parameters in the model. It must be determined interactively during the running of the calculation by monitoring the size of $\delta\underline{g}$ in Eq. (A42). Unfortunately, the frequency with which we must update $\underline{g}$ increases with β because the matrix $\underline{I}+\underline{b}(l,i)$ becomes badly conditioned as β becomes large. This is why we were unable to carry the Monte Carlo calculations to very low temperatures.

[1]T. D. Lee and C. N. Yang, Phys. Rev. **87**, 410 (1952).
[2]D. C. Jou and M. M. Chen, J. Phys. C **6**, 2713 (1973).
[3]R. Blankenbecler, D. J. Scalapino, and R. L. Sugar, Phys. Rev. D **24**, 2278 (1981); D. J. Scalapino and R. L. Sugar, Phys. Rev. B **24**, 4295 (1981).
[4]Some Monte Carlo results for the 2D classical lattice gas with $V>0$ have been published: D. J. Scalapino, R. L. Sugar, and W. D. Toussaint, Phys. Rev. B **29**, 5253 (1984).
[5]M. E. Fisher and M. N. Barber, Phys. Rev. Lett. **28**, 1516 (1972); M. N. Barber, in *Phase Transitions and Critical Phenomena,* edited by C. Domb and J. L. Lebowitz (Academic, New York, 1983), Vol. 8.
[6]J. de Boer, Physica **14**, 139 (1948).
[7]H. A. Kramers and G. H. Wannier, Phys. Rev. **60**, 252 (1941).
[8]J. M. Kosterlitz and D. J. Thouless, J. Phys. C **6**, 1181 (1973).
[9]L. Van Hove, Phys. Rev. **89**, 1189 (1953).
[10]J. Hirsch [Phys. Rev. B **31**, 4403 (1985)] has found similar effects for the 2D Hubbard model (unpublished).
[11]J. Hirsch and D. J. Scalapino, Phys. Rev. B (to be published).
[12]See Ref. 2, and references contained therein.
[13]H. Kawamura, Prog. Theor. Phys. **68**, 764 (1982); **68**, 1026 (1982). Kawamura has studied a quantum lattice gas with infinite-range interactions and concluded that the 2D half-filled square lattice has T_c going to zero at a finite value of the interaction. However, we believe this is incorrect, and that our RPA results are appropriate for such a system.
[14]J. Hirsch, Phys. Rev. B **28**, 4059 (1983).